Diamond & Related Materials 72 (2017) 61–70

Contents lists available at ScienceDirect

Diamond & Related Materials

journal homepage: www.elsevier.com/locate/diamond

Express *in situ* measurement of epitaxial CVD diamond film growth kinetics

E.V. Bushuev [a], V.Yu. Yurov [a,b,*], A.P. Bolshakov [a,b], V.G. Ralchenko [a,b,c], A.A. Khomich [a,b], I.A. Antonova [a,b], E.E. Ashkinazi [a,b], V.A. Shershulin [a,b], V.P. Pashinin [a], V.I. Konov [a,b]

[a] A.M. Prokhorov General Physics Institute of Russian Academy of Sciences, Moscow, Russia
[b] National Research Nuclear University "MEPhI", Moscow, Russia
[c] Harbin Institute of Technology, Harbin, PR China

ARTICLE INFO

Article history:
Received 13 November 2016
Received in revised form 23 December 2016
Accepted 31 December 2016
Available online 3 January 2017

Keywords:
Single crystal diamond
Microwave plasma CVD
Interferometry
Etching
Optical emission spectroscopy

ABSTRACT

We used a low-coherence interferometry for precise continuous *in situ* measurements of thickness and growth rate of epitaxial single crystal diamond layers in microwave plasma CVD in H_2-CH_4 gas mixtures in a broad range of substrate temperatures T_s (750–1150 °C) and CH_4 concentrations (1–13%). Rich growth kinetics is collected in a single experiment by depositing about 60 layers on one (100) Ib HPHT diamond substrate in different regimes (the substrate temperature was controlled by the microwave power) at fixed pressure $P = 130$ Torr, without the plasma switch-off. The growth rate is found to follow Arrhenius dependence with activation energy $E_a = 11.1 \pm 1.0$ kcal/mol. By appropriate choice of the substrate temperature the growth rate can be significantly enhanced. The growth rate as high as 82 μm/h is achieved by optimizing the temperature and gas composition. At low CH_4 content (1%) growth competes with etching by atomic hydrogen, the etching dominating at high T_s (>1000 °C in the present conditions). The etching rate in pure H_2 plasma was measured and activation energy $E_a = 9.8 \pm 0.8$ kcal/mol was deduced. Gas temperature T_g in the plasma core evaluated from optical emission spectra for dimer C_2 (Swan band), was found to be either constant or slightly and monotonically increasing with absorbed power, whereas the absorbed microwave power density shows a decreasing, although slight, trend. This suggests the temperature depended surface reactions to play a major role in the diamond growth kinetics under variable microwave power. Raman mapping of cross-section of the produced multilayered sample confirmed high quality of diamond structure over all the deposition regimes explored.

1. Introduction

The increasing interest in single crystal (SC) diamond produced by microwave plasma assisted chemical vapor deposition (MPCVD) for advanced applications such as radiation-hard detectors [1,2], Raman lasers [3], electronic devices [4,5], quantum technologies based on color centers in diamond [6], demands an optimizing of the diamond synthesis process *via* enhancement in growth rate while keeping high quality of the material, and a better control (stabilization) of the growth process itself. The growth rate can be enhanced by increasing the concentration of active radicals, like CH_3, and atomic hydrogen in gas [7] and/or by control surface reactions rate, for example, by changing the substrate temperature or adding chemically active species. The first approach relies on increasing of operating pressure [8–10], absorbed microwave power density [11,12], methane content in process gas [13], or adding an inert gas, like Ar, to reduce thermal conductivity in plasma [14,15], while the latter methods use small addition of N_2 in gas mixture [16–18] and substrate temperature variation. There are, however, only limited experimental data on dependence of growth rate of SC diamond on substrate temperature in MPCVD process [9,17,19–21]. Achard et al. [20] obtained epitaxial films at fixed CH_4 concentration (4%) and different substrate temperatures ranging from 800 °C to 950 °C, and found a maximum in growth rate around $T_s = 875$ °C. They noted a complex combined effect of nitrogen addition and T_s increase for the growth rate and surface morphology. The same group reported also a monotonic growth rate with temperature in the range of 750 °C to 950 °C for different faces, including (100), (110), (111) and (113), at 4% CH_4 [17]. Lu et al. [9] measured the dependence of growth rate *vs* substrate temperature $G(T_s)$ for moderate CH_4 concentrations of 4 to 7%, and defined a window in T_s of 1030 to 1250 °C, where a maximum growth rate is achieved. Moreover, the best diamond quality was assessed from Raman spectra for the materials produced at the highest rate. Yamada et al. [21] studied $G(T_s)$ dependence for epitaxy on large-area 20 × 40 mm^2 mosaic SC CVD substrates in gas mixtures consisting of hydrogen with typically 5% of methane, and obtained a

* Corresponding author at: A.M. Prokhorov General Physics Institute RAS, Vavilov str. 38, Moscow 119991, Russia.
E-mail address: yurov6591@gmail.com (V.Y. Yurov).

http://dx.doi.org/10.1016/j.diamond.2016.12.021
0925-9635/

weak maximum around $T_s \approx 1030$ °C. The gas mixtures with low CH_4 contents (typically below 4%) and very high ones (>8–10%) were not addressed in the previous temperature optimization studies. A brief review of early works on the substrate temperature effect on growth rate on SC diamond films was given by Teraji [19].

Here, we report on precise continuous *in situ* measurements of the thickness and growth rate of epitaxial single crystal diamond layers by microwave plasma CVD in H_2-CH_4 gas mixtures in a wide temperature range of 750–1150 °C and methane content of 1–13%, using a low-coherence interferometry (LCI) [22]. The low-growth-rate regimes at low CH_4 contents, typically of <1%, are important for producing atomically flat surfaces [23,24] and high quality SC for radiation detectors [25], while high growth rates can be achieved at elevated CH_4 concentrations in process gas [9,15,16,26]. The geometry of MPCVD chamber in our ARDIS-100 system, with quartz microwave window positioned far from the plasma region [15], allows the use of H_2-CH_2 gas mixtures with high methane contents, well above 10%, which is difficult to exploit with MPCVD systems of bell-jar type due to soot deposition on the quartz dome. The moving to CH_4-rich mixtures provides one of the means to further increase the growth rate. The *in situ* control of the growth rate with LCI used in the present work can greatly accelerate the multiparametric study of diamond growth regimes. It is able to reduce collection time of the experimental kinetic data to few hours only as compared to more commonly used approaches based on preparation of many samples and *ex situ* characterization, the whole procedure typically taking weeks and even months.

2. Experimental

The growth of SC diamond films was performed using a MPCVD system ARDIS-100 (Optosystems Ltd., 5 kW, 2.45 GHz) as described elsewhere [15,22]. A mechanically polished (100) oriented type Ib commercial HPHT diamond plate with dimensions of $3.5 \times 4.5 \times 0.72$ mm^3 was used as the substrate. Before the diamond deposition the substrate was pretreated in H_2/O_2 microwave plasma (70 Torr, 2300 W, 2 h) to etch away surface defects such as dislocations and those caused by polishing [27,28]. The epitaxial growth then has been performed using H_2-CH_4 mixtures at pressure $p = 130$ Torr and total flow rate $Q = 500$ sccm in the temperature range of 750–1150 °C for methane contents varied from 1 to 13%. The purity of source gases was 99.99999% for H_2, 99.9995% for CH_4. The desired substrate temperature T_s was established through the microwave power P tuning in the range of 1.8–3.3 kW. The temperature was determined by a two-color IR pyrometer (Micron Instruments, model M770) looking on the edge of the sample *via* a side quartz viewport of the CVD chamber (the diameter of thermal emission probed area of ≈ 2 mm). Preliminary, a black polycrystalline diamond rim with high emissivity was formed on the substrate by diamond deposition at 10% CH_4 content in a few hours to stabilize the pyrometer reading and to make further temperature measurements more reliable. The CVD diamond epilayer of ≈70 μm was formed during this pregrowth.

Real-time measurements of the thickness and growth rate of the epitaxial films were performed with a low-coherence Michelson tandem-type interferometry (LCI) that we recently introduced in practice [22]. In brief, the beam of the low-coherence infrared radiation from a superluminescent diode (SLD) at $\lambda_0 = 1560$ nm wavelength with bandwidth $\Delta\lambda = 30$ nm, was directed perpendicularly to diamond sample surface through an objective of the interferometer positioned above the 10 mm thick upper quartz window of the CVD chamber. The LCI system is able to measure the temporal evolution of optical thickness $nd(t)$ of the growing sample, where n is refraction index of diamond, and d is the total sample thickness (substrate plus film). The nd values are collected with frequency of ≈0.3 Hz. The growth rate G is found as the time derivative of the increment in optical thickness $\Delta(nd)/n_0\Delta t$, where $n_0 = n(T = 950\,°C) = 2.43$ is refraction index at the average temperature of the temperate range studied. The values $n(T)$ and $d(T)$ are the temperature depended, and for accurate measurements this should be taken into account. Typically, <10 min growth run was required to get enough data points to evaluate the growth rate with high accuracy at given temperature. Then, the sample temperature received a small increment, and the next layer was deposited on the previous one. Thus, the eventually produced multilayer sample contained kinetic information about several tens different growth regimes.

The method used here to vary the substrate temperature *via* the choice of appropriate value of microwave power is justified to some extent by the finding of Lu et al. [9] that the absorbed power density P/V, where V is the plasma volume, only weakly depends on the absorbed MW power P (we did confirm this trend in present work, see Section 3.5). This gives an indication that the gas temperature (T_g) and the plasma chemistry might also change only slightly with incident MW power, and the measured growth kinetics $G(T_s)$ will reflect primarily the substrate temperature effect, rather than variation of radical composition in the plasma.

The plasma volume V was calculated by mapping the hydrogen H_α line optical emission intensity $I(H_\alpha)$. Since the upper level of the H_α line is excited by electron impact, the intensity $I(H_\alpha)$ is proportional to electron concentration n_e, so the $I(H_\alpha)$ profiling allows estimate the plasma dimensions [29]. The photographs of the plasma cloud were captured with a digital mirror camera Canon EOS 650D through a red H_α–filter passing only the H_α line emission ($\lambda = 656.5$ nm ± 6 nm). The spatial profiles of the H_α line emission along X (parallel to the substrate surface) and Z (perpendicularly to the substrate surface) axes were then determined from the images, and the shape of the plasma was very well fitted with 3D Gaussian profiles, with further estimation of the volume and calculation of microwave power density (MWPD) values.

Panoramic optical emission spectra (OES) of the plasma were recorded with Ocean Optics HR4000 spectrometer equipped with a grating with 600 lines/mm (wavelength range of 400–800 nm, spectral resolution 0.6 nm). High resolution OES for the plasma (H_α, H_β, H_γ, CH and C_2 lines) were measured with a M833 spectrometer (Solar Laser System, focal length of 833 mm, spectral resolution of 0.01 nm), equipped with a double grating with 2400 lines/mm and CCD image sensor Hamamatsu S10420-1006. The emission spectra were taken within the central area of the plasma ball in horizontal direction, with spatial resolution of ~1.5 mm, using an optical fiber system [15]. The gas temperature was evaluated from OES data measured in the central region of plasma (horizontal cylinder with ≈10 mm diameter) by the analysis of the (0,0) band of the C_2 Swan system ($d^3\Pi_g \rightarrow a^3\Pi_u$) with spectral resolution of 0.01 nm, following the procedure described in [30,31]. Here, a thermal equilibrium between heavy species' translational and rotational modes, and a Boltzmann distribution of the rotational levels of the considered vibrational state are assumed. The measured rotational temperature was taken as the gas temperature T_g.

The produced multilayer diamond sample was characterized by Raman and photoluminescence spectroscopy using LabRam HR800 (Horiba Jobin-Yvon) spectrometer in a confocal configuration with spectral resolution of 2.0 cm^{-1}, dispersion 0.59 cm^{-1} and spatial resolution of ~1 μm. The excitation laser beam ($\lambda = 473$ nm) was focused on the sample top surface, and the light from the sample was collected in backscattering geometry with microscope objective (Olympus, magnification ×100, numerical aperture NA = 0.90). The surface topography and surface roughness of the epilayers were measured with atomic force microscopy (Ntegra Spectra, NT-MDT Ltd), and optical profilometry (NewView 5000, ZYGO).

3. Results and discussion

3.1. Temperature control

The dependence of substrate temperature T_s on absorbed microwave power $P = P_{incident} - P_{reflected}$ is shown in Fig. 1. The variation of T_s from 750 to 1150 °C is achieved when the MW power P spanned from 1.8 to

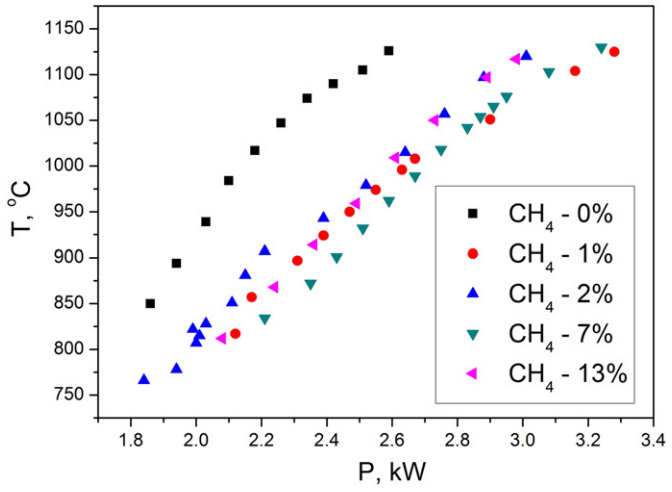

Fig. 1. The dependence of substrate temperature T_s on absorbed microwave power P for different CH_4 percentages in gas. The $T_s(P)$ curve for pure H_2 plasma is also shown (squares).

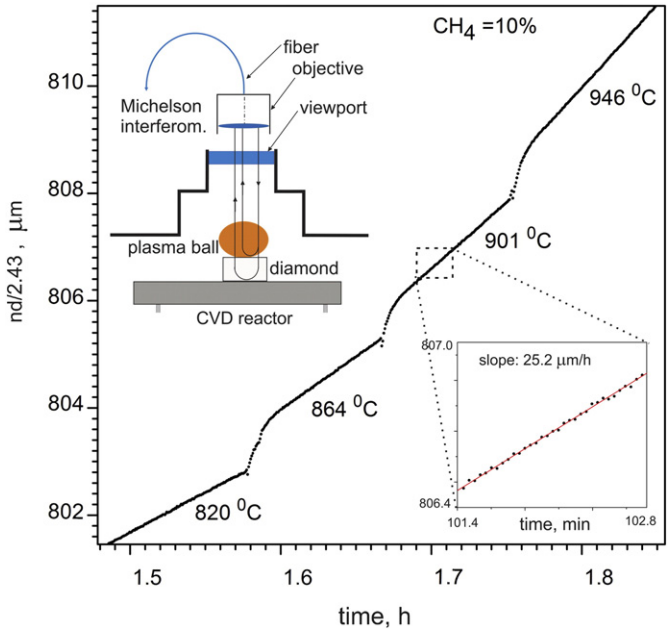

Fig. 2. Evolution of epilayer thickness with time under consecutive rise in steps of substrate temperature at 10% CH_4 content as measured with LCI. The temperature is indicated for each segment. The linear segments correspond to the growth with constant rate. The transitions between two segments are due to temperature dependence in $n(T)d(T)$ product. Insets: a detail of the plot illustrating the number of measured data on a selected segment and the linear fit to the data (on right bottom); optical scheme of LCI measurements of sample thickness (on left top).

3.3 kW. The temperatures below 750 °C were not attained due to the plasma instability at low power ($P < 1.8$ kW), while the maximum T_s value was limited by the pyrometer temperature range. With the CH_4 content varied in the range of 1 to 13%, the $T_s(P)$ curves display quite similar trend for all CH_4 percentages, being confined in narrow corridor. This makes convenient the substrate temperature tuning for different gas compositions within the same power range. The substrate is heated stronger (by 100–150 °C) in pure hydrogen (see the upper curve in Fig. 1) provided the same powers are compared. The relative cooling of the substrate upon CH_4 adding can be assigned to a change in ion composition in comparison with the H_2 plasma, as studied experimentally and with a modeling by Ma et al. [29]. They found that neither the atomic hydrogen in ground state H ($n = 1$) concentration nor the H_2 dissociation fraction is sensitive to CH_4 content, however, the dominant ion of the plasma switches from H_3^+ to $C_2H_3^+$ and $C_2H_2^+$ upon adding CH_4 in contents just below 1%. These hydrocarbon ions have lower mobility than H_3^+, leading to the plasma shrinkage. The reduced thermal and radiation emission fluxes towards the substrate cause the observed drop in T_s when even a small CH_4 concentration is added in H_2 (Fig. 1).

3.2. Growth rate measurements

The growth experiment started from the substrate heating in pure H_2 at lowest power of 1.8 kW, then methane at fixed concentration was introduced in the reactor, and for a few minutes the substrate temperature T_s was stabilized at low level of 750–800 °C. To determine the growth rate the linear increase in thickness was monitored by interferometry for a certain time, then the power was increased by a small value to establish a higher T_s level, and the growth rate measurement was repeated. Fig. 2 shows for particular gas composition (10% CH_4) how the effective diamond film thickness $n(T)d(T)/n_0$ changes with process time. In this part of the experiment the temperature was changed in steps three times to cover the range of 820 to 946 °C for the time interval of 17 min, to determine the growth rate at each T_s. Here, the diamond refraction index $n_0 = 2.43$ at $\lambda = 1560$ nm, as extrapolated from [32] was taken at $T = 950$ °C, the middle between the lowest and highest temperatures used in the present work, to convert the measured optical thickness to the effective thickness. After a steep increase of microwave power the temperature responses by an increase for approximately 40 s to a new equilibrium, that manifests itself in a step in nd/n_0 value as seen in Fig. 2. The steps in the measured thickness are due to the fact that both $n(T)$ and $d(T)$ are increasing functions of the temperature [33,34], therefore the apparent stepped increment in $nd(t)$ is mostly of the thermal nature, rather than reflects a real film deposition. The change in power translates to the temperature very quickly, then a linear increase of $nd(t)$ with time is observed, and the growth rate is determined from the slop. Typically 5 to 10 min of the linear growth time was enough to determine the growth rate at fixed T_s with high accuracy. As an example, the inset in Fig. 2 shows a part of a highly linear $nd(t)/n_0$ dependence for the temperature $T_s = 901$ °C with 34 data points. The linear fit to the data for the whole segment (100 data points) by least-square method gives the slop 25.2 ± 0.03 μm/h, that indicates the high accuracy of ~0.1% in assessment of growth rate.

The surface roughness R_a can limit the accuracy of the measured thickness, for example, at $R_a = 100$ nm and the sample thickness $h = 500$ μm the error is $R_a/h \approx 0.02\%$. However, the error in the growth rate seems to be less sensitive to the roughness, if the surface relief does not change essentially over short measurement time, so all parts of the surface within 40 μm diameter area probed by LCI, get identical thickness increment. This makes possible a reduction in error (<0.1%) even for thin or rough samples. The main practical error in the growth rate evaluation is caused by the sample temperature fluctuations or drift, which directly change the apparent $n(T)d(T)$ product. We estimate the growth rate error of ≈0.1 μm/h for the temperature drift $\Delta T = \pm 1$ °C during six minutes of the LCI measurement procedure, that could be essential at slow growth ~1 μm/h. For this reason the microwave power was tuned manually in some cases to better stabilize the temperature.

Taking into account the linear temperature dependence for $n(T)$ between 750 and 1150 °C [32,33] and the value of $(dn/dT)/n \approx 8 \times 10^{-6}\ K^{-1}$ for thermooptical coefficient at 950 °C, we estimate the maximum change in the refraction index at the temperature variation ΔT of ±200 °C to be very small, $\Delta n = n_0[(dn/dT)/n]\Delta T \approx 3.9 \cdot 10^{-3}$. Thus, using of average refraction index n_0 in the temperature range of interest allows determination of the geometrical thickness of the sample $d = nd/n_0$ with the error <0.4%.

The common way to determine the growth rate *ex situ* is the measurement of the sample thickness before and after the deposition run ("cold" growth rate), and this is done at room temperature (RT). Note, that actually we measure here a "hot" growth rate G_{hot}, as the

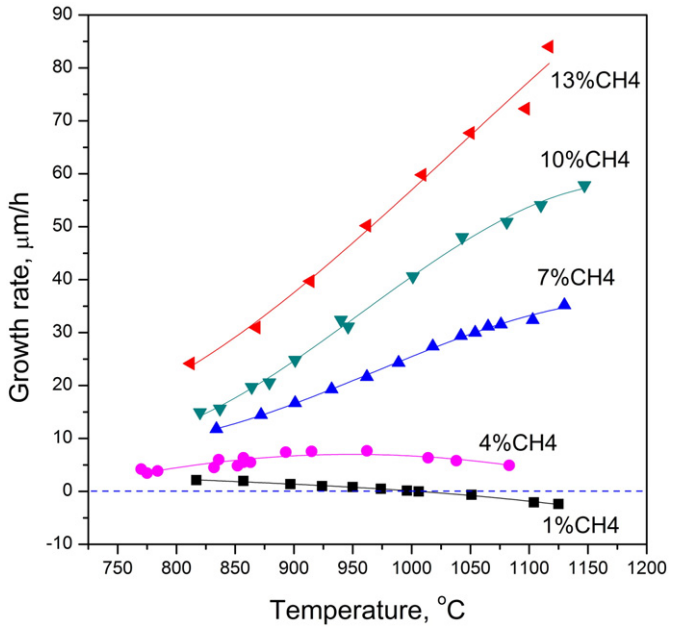

Fig. 3. Dependence of growth rate on substrate temperature $G(T)$ at different CH_4 contents in gas mixture. Note the net etching for 1% CH_4 at $T_s > 1000$ °C.

monitored effective thickness increment refers to the growth temperature, rather than to RT. The "hot" growth rate exceeds the "cold" (*ex situ*) growth rate by a value of $\Delta G = \langle\alpha\rangle \times \Delta T \times G$, where $\Delta T = T_s - 25$ °C, and $\langle\alpha\rangle \approx 3 \times 10^{-6}$ K^{-1} is the thermal expansion coefficient for diamond averaged over the temperature range ΔT. This difference ΔG related to thermal expansion is, however, quite small (~0.3%), and we neglect it in further consideration.

Temperature dependences of growth rate $G(T)$ for different CH_4 contents in process gas reveal several trends as shown in Fig. 3. First, the maximum growth rate at given T_s increases with adding more methane in gas. Second, at low CH_4 contents a maximum in $G(T)$ at certain temperature T_{max} is observed: for 4% CH_4 it is seen at 950 °C, and for 1% CH_4 it lies below 800 °C. Third, the $G(T)$ plots for moderate CH_4 concentrations (7 and 10%) demonstrate a different pattern: the growth rate strongly and monotonically increases with T_s, with indication to a saturation or maximum near 1150 °C, while no sign of such saturation can be seen for $G(T)$ curve for the most methane-reach mixture (13% CH_4). This observation is in agreement with the data of Lu et al. [9], who found the maximum growth rate to occur at $T > 1150$ °C at methane contents of 5–7%. We conclude that the growth rate can be strongly improved by optimizing the substrate temperature. The maximum in growth rate occurs due to two factors. First, at high temperatures desorption of CH_3 and C_2H_2 species becomes more rapid, and competes with the carbon incorporation reactions, as follows from diamond growth process simulation [35]. Second, the $G(T)$ dependence decline is aggravated by enhanced etching by atomic hydrogen of the plasma at high temperatures. Interestingly, for 1% CH_4 the etching effect prevails at $T > 1000$ °C, so the net decrement in the film thickness was revealed, and negative growth rate was observed (the results on etching in pure H_2 plasma see in more detail onward in Fig. 7).

By vertical sections of the curves on $G(T)$ in Fig. 3 the data have been re-plotted to demonstrate growth rate dependence on methane concentration in gas at different T_s (Fig. 4). For any CH_4 percentage, from the 1% to the highest, 13%, the $G(CH_4)$ increases monotonically. Recently [15], we reported the growth rate *vs* CH_4 content at fixed $T_s = 965 \pm 15$ °C using the same ASRDIS-100 system and *ex situ* thickness measurement. The present result (the data for 950 °C in Fig. 4) agrees very well with the previously obtained $G(CH_4)$ dependence (see also Fig. 5), particularly, the growth rate is 43 μm/h and 45 μm/h at 13% CH_4 for *ex situ* and *in situ* measurements, respectively, in the independent growth events.

It's instructive to compare the achieved maximum growth rates (within the temperature range explored in present work) at different CH_4 contents with those obtained at a fixed T_s. Fig. 5 compares the maximum growth rate G_{max} as function of CH_4 content (as deduced from Fig. 3) with the growth rates achieved at 950–980 °C (this temperature is optimized for 4% CH_4) at the same pressure $p = 130$ Torr in our previous study [15], with very similar other process parameters. By appropriate choice of the substrate temperature it's possible to almost double the growth rate compared to that at the fixed T_s, especially for the gas mixtures enriched with methane. The growth rate as high as 82 μm/h is achieved at the 13% CH_4 by increasing the temperature to 1147 °C.

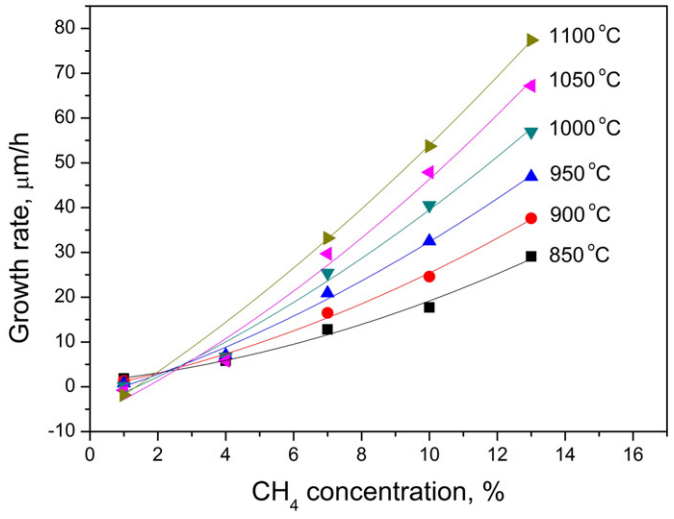

Fig. 4. Dependence of growth rate on methane concentration in gas at different substrate temperatures.

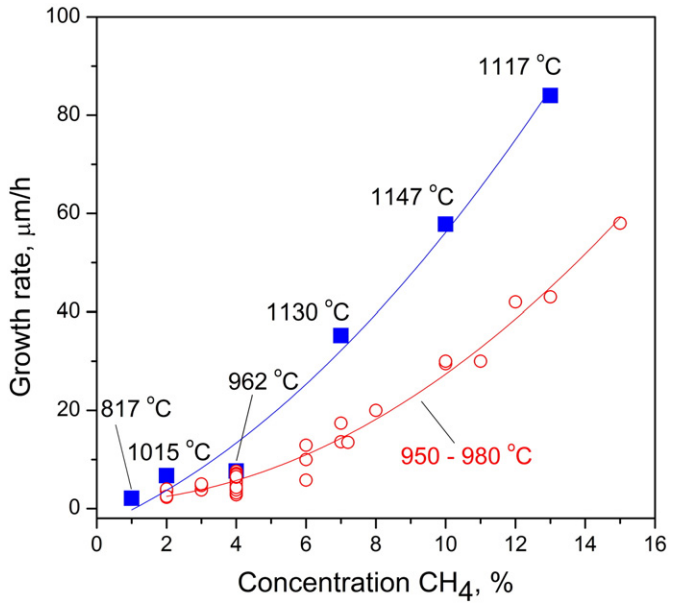

Fig. 5. Dependence of maximum growth rate G_{max} on CH_4 content in gas (squares). The corresponding temperature T_{max} for G_{max} is indicated for each data point. The measured $G(\%CH_4)$ plot at fixed substrate temperature 965 ± 15 °C and $p = 130$ Torr [15] (circles) is shown for comparison.

3.3. Growth activation energy

Assuming the reaction rate can be described with an Arrhenius-type equation $G(T) = B \times \exp(-E_a/RT_s)$, where $R = 1.987$ kcal/mol K is universal gas constant, T_s is the absolute substrate temperature, and B is a constant, the Arrhenius plots $\ln(G) \sim 1/T$ for rising parts of growth rate temperature dependences were composed, which are displayed in Fig. 6 for CH_4 concentrations of 7, 10 and 13%. The activation energy E_a determined from the slop ranges from 10.2 ± 0.8 kcal/mol for 7% CH_4 to 12.2 ± 1.0 kcal/mol for 10% CH_4, the value for 13% CH_4 being in between (11.8 ± 0.9 kcal/mol). It was difficult to determine the activation energy for low-CH_4 mixtures because of a limited number of data points presented on the corresponding rising parts of $G(T)$ curves.

The experimental data on E_a are scarce in literature. Maeda et al. [36] reported the apparent activation energy of 7.4–15.2 kcal/mol for growth on (100) face at low temperatures 650–750 °C and low CH_4 percentage of 0.5–2.0%. Chu et al. [37] have determined activation energy $E_a = 8 \pm 3$ kcal/mol for hot-filament deposition on (100) face at a methane mole fraction of 0.4% at substrate temperatures between 735 and 970 °C. When the combustion flame method was applied for homoepitaxial diamond growth using acetylene as the source gas, E_a was reportedly 12 kcal/mol for the (100) crystal plane at $T_s = 1000$–1400 °C [38]. In spite of quite different growth process parameters in the present work with those used by the other authors, the average activation energy of 11.1 ± 1.0 kcal/mol (≈46 kJ/mol) found by us is in a reasonable agreement with those previous results. The accuracy of ≈8% for activation energy determined here, is much better than that ever reported before, as the *in situ* technique provides more data points for analysis.

The diamond growth on (100) face was simulated in a number of works and activation energy of the surface reactions involved have been deduced [7,39,40]. The density functional theory (DFT) calculations [39] gave a set of activation energy values E_a associated with various elementary steps for CH_2 incorporation into the C—C dimer bond, the latter considered as the primary growth mechanism. Hydrogen abstraction corresponds to $E_a = 26.4$ kJ/mol, while CH_2 radical (formed by H abstraction from CH_3) incorporates into the diamond structure *via* a ring opening/closing sequence with activation energy of 28.0 kJ/mol, other steps proceeding without a barrier. Thus, the experimental data for E_a exceed by a factor 1.6 those obtained from that particular modeling. This may indicate the description of the measured growth kinetics by a single exponent to be too simplified approach, yet it gives a practical guide to predict the temperature sensitivity of growth rate.

3.4. Etching effect

At low CH_4/H_2 ratios the growth rate can be comparable to etching rate by atomic hydrogen, so the measured $G(T)$ dependence is a result of competition in growth/etching processes [35]. To quantify the etching rate it was measured as function of substrate temperature in pure H_2 plasma at pressure $p = 130$ Torr and flow rate of 500 sccm for the same multilayer CVD diamond sample, immediately after the deposition of top layer at 13% CH_4. Fig. 7 shows the temperature dependence of the etch rate R_{etch} in the range of 850 to 1125 °C. The etch rate R_{etch} is about 1.5 μm/h at 850 °C, and increases with T_s to 6.0 μm/h at the highest temperature. The growth rate dependence $G(T)$ for 1% CH_4, also shown here for comparison, demonstrates a continuous decline as a result of the etching process enhancement. The etching and growth rates become equal at $T \approx 1000$ °C, the etching dominating at higher temperature. Slightly below this transition temperature the growth rate can be as low as a few nanometers per minute, still well controlled, that could be interesting for deposition of superthin diamond epilayers for electronic devices or 2D arrays of single photon emitters on color centers. Due to the very low growth rate the deposition process can be realized in conventional CVD reactors, without pulsed feed of the reactants to the substrate zone.

The etching rate can be described by Arrhenius equation $R_{etch} = A \times \exp(-E_a/RT_s)$, where A is a constant, and we found $E_a = 9.8 \pm 0.8$ kcal/mol from the slope in the Arrhenius plot in Fig. 8. This activation energy is much less than the value $E_a = 45.4 \pm 4.5$ kcal/mol reported by Ivanov et al. [41] for etching of (100) oriented Ib type HPHT diamond in H_2 microwave plasma in similar conditions ($p = 130$–150 Torr, 3.5 kW, $T_s = 800$–1100 °C). Also, the absolute etch rate for the HPHT diamond [41] (<90 nm/h at 950 °C) is an order of magnitude lower than that in our measurements (1.9 μm/h at 950 °C). So big distinction in E_a and the etch rates could be due to a difference in surface topography of CVD diamond films, which is very complex, with terraces and steps (see further Section 3.7 and AFM images in Fig. 15), and the polished HPHT single crystal sample etched in the work [41], and/or due to a difference in defects abundance in the compared samples. If surface

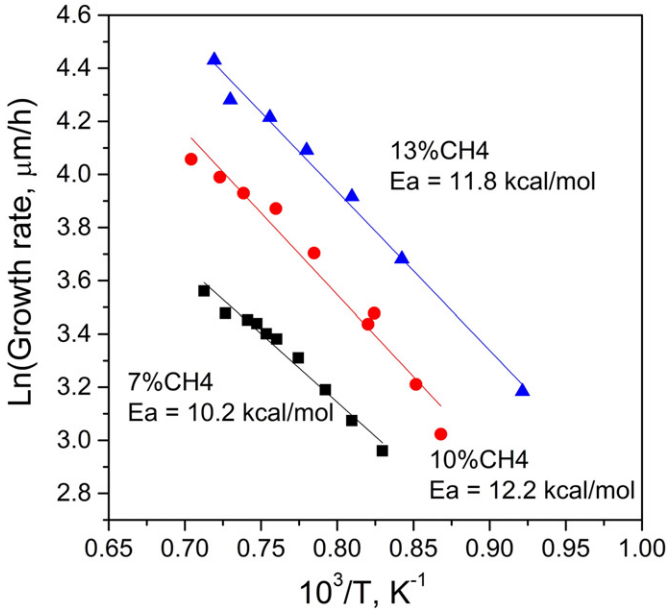

Fig. 6. Arrhenius plot for growth rate $G(T)$ at different CH_4 concentrations of 7% (squares), 10% (circles) and 13% (triangles).

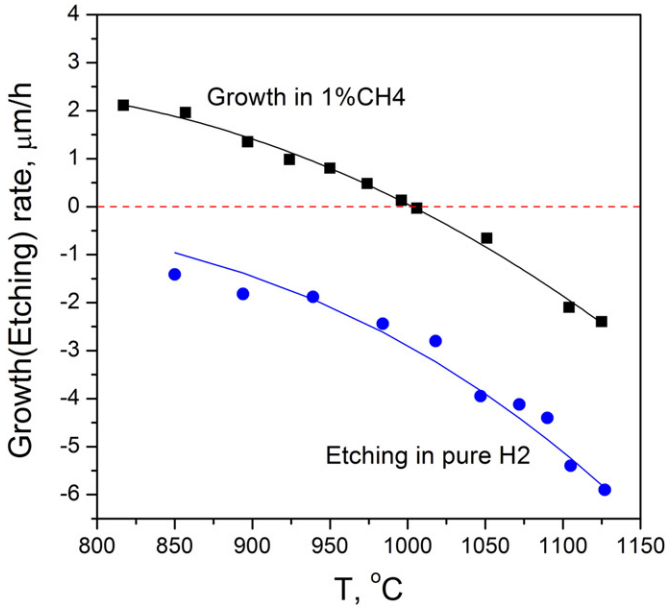

Fig. 7. Etching rate $R_{etch}(T)$ in pure H_2 (circles) and growth rate $G(T)$ at 1% CH_4 (squares) *vs* substrate temperature. The symbols are experimental data, the lower line is fitting of etch rate by exponential function $R_{etch} = A \times \exp(-E_a/RT_s)$.

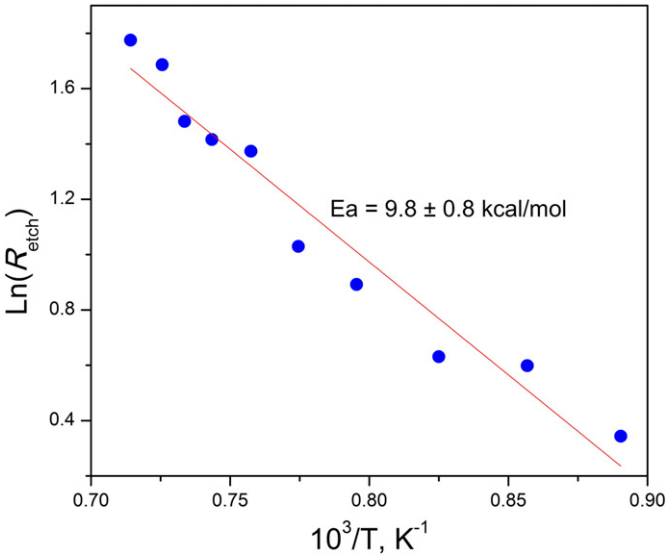

Fig. 8. Arrhenius plot for etching rate in pure H_2 plasma at $p = 130$ Torr.

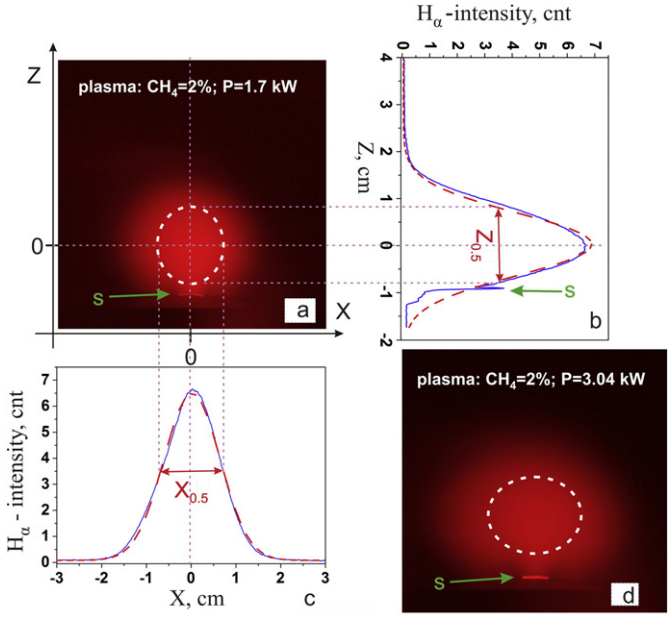

Fig. 9. Photo of plasma through a H_α-filter (a) and (d) at different growth parameters ($CH_4 = 2\%$; $P = 1.7$ and 3.04 kW, respectively). Appropriate profiles of H_α-intensity for photo (a) is shown in X and Z direction shown by blue lines on (b) and (c); dashed red lines on the profiles denote Gaussian fits. White dashed ellipse on (a) and (d) shown area where H_α-intensity is equals to $0.5 \times I(H_\alpha)_{max}$. Green arrows on images and profile (d) indicate position of the substrate.

migration along the terrace of radicals participated in etching is taken into account, the enthalpy change upon etching will depend on position of carbon atom to be desorbed, at the edge of the step or in the midst of surface terrace [35,41]. A further study of etching kinetics is needed to elucidate the etching mechanism, in particular, at lower temperatures, where the error in etch rate in our present measurement was significant. The issue of a potential correlation between the measured etching rate and specific surface relief of SC diamond films could be an interesting topic for a future work. In the present experiment this was, however, principally impossible since all the deposited layers, except the last one, were buried.

3.5. Microwave power density

The microwave power density P/V determines elementary processes and concentration of species in the plasma (assuming other parameters, such as pressure, feed gases, to be fixed) [42]. A constancy (if takes place) of the microwave power density (MWPD) upon the absorbed power variation would suggest a stability of plasma chemistry and radials flux towards the growing diamond surface. This, in turn, would give a ground to consider the observed temperature dependencies of growth rate to be the result of solely surface chemistry, rather than of a combined effect of the plasma chemistry and the substrate temperature variations. Indeed, Lu, et al. [9] found only weak dependence of MWPD on the absorbed power in their bell-jar CVD system. When the input power increased the discharge volume also increased, thereby the MWPD value remained approximately constant, or decreased slightly, demonstrating a kind of a self-consistent process. Here we measured the MWPD as function of absorbed power for different CH_4 concentrations and observed a similar trend. The plasma volume was evaluated by profiling atomic hydrogen H_α line intensity on images captured with a digital mirror camera (Canon EOS 650D) through a H_α-filter, that passed only the H_α line emission in the plasma spectra. It was necessary to save images as a RAW-data, that keep linearity in intensity in the photo, and allow measurements of X and Z profiles for the H_α line emission. An approach to estimate MWPD from photographic plasma images with H_α-filtering was described previously by Lobaev et al. [45]. As an example, the plasma images in H_α emission at MW power of 1.7 and 3.04 kW are displayed in Fig. 9. The plasma cloud expands with the MW power increase, keeping elliptical shape. The X-profile for $I_{H\alpha}(X)$ was fit with a Gaussian profile, and similar Gaussian fitting was found satisfactory for Z profile.

An Abel inversion procedure [43,44] was applied to the $I_{H\alpha}(X)$ profiles in order to obtain the radial distribution of the local emissivity $I_{H\alpha}(R)$, which turned out to have the Gaussian shape as well, with the same width (FWHM) $\Delta X_{0.5}$. The comparison of experimental X and Z profiles for H_α line and the corresponding Gaussian fits for the two microwave powers are demonstrated in Fig. 9.

Due to axial symmetry of chamber and discharge in Z direction the emission spatial profile $I_{H\alpha}(x,y,z)$ is described with a 3D Gaussian function ($Y_{0.5} = X_{0.5}$):

$$I_{H\alpha} = I_0 \times \exp^{-\left(\frac{x^2+y^2}{2s_x^2}\right)} \times \exp^{-\left(\frac{z^2}{2s_z^2}\right)} \quad (1)$$

where $s_x = X_{0.5}/[2\sqrt{(2\ln 2)}]$, $s_z = Z_{0.5}/[2\sqrt{(2\ln 2)}]$, and $I_0 = I_0(0,0,0)$ is the intensity in center of the plasma cloud, which is not necessarily spherical. Then the plasma volume can be calculated by an ellipsoid formula:

$$V = \pi(\Delta X_{1/e})^2 \times \Delta Z_{1/e}/6 \quad (2)$$

where $\Delta Y_{1/e} = \Delta X_{1/e} = \Delta X_{0.5}/\sqrt{(\ln 2)} \approx 1.44 \times \Delta X_{0.5}$ and $\Delta Z_{1/e} = \Delta Z_{0.5}/\sqrt{(\ln 2)} \approx 1.44 \times \Delta Z_{0.5}$ are the widths corresponding to $I_{H\alpha}$ drop from maximum to I_0/e level (e = 2.718). The power density P/V dependences on adsorbed MW power for low (2%) and high (10%) CH_4 contents in gas are displayed in Fig. 10. The MWPD decreases from ≈420 ÷ 490 to ≈300 W/cm^3 with absorbed power increase in the range of 1700 to 3000 W, with the similar trends for both 2% and 10% CH_4 curves. The difference in MWPD for the two CH_4 concentrations is <20% within the MW power range explored. For moderate and higher powers of 2400–3100 W the power density is almost constant.

3.6. Plasma temperature

A further insight in MW power effect on plasma parameters has been provided with gas temperature measurements in the central

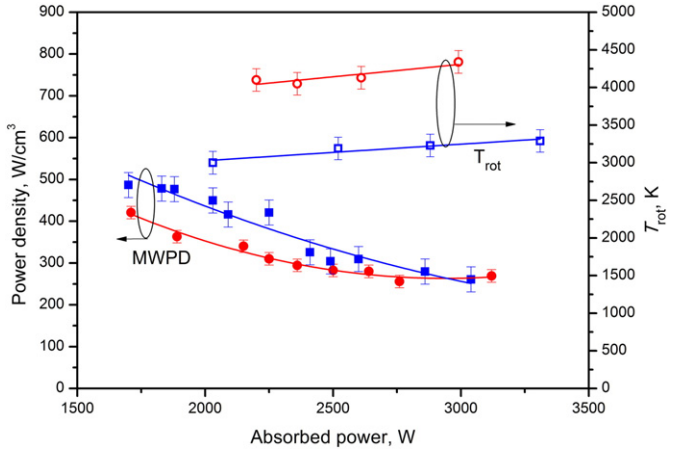

Fig. 10. Left vertical axis: MW power density $\rho = P/V$ *vs* absorbed MW power P at concentrations 2% CH_4 (full squares) and 10% CH_4 (full circles) in H_2. Right vertical axis: rotational temperature in the core of plasma cloud measured from C_2 emission spectrum at 2% CH_4 (open squares) and 10% CH_4 (open circles). Pressure $p = 130$ Torr.

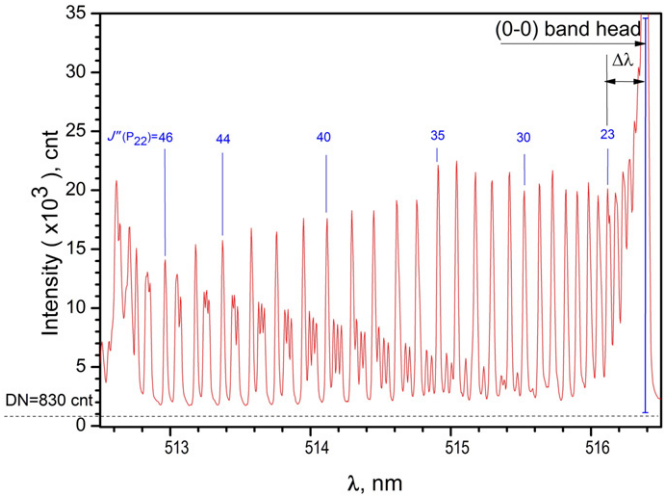

Fig. 12. High resolution optical emission spectrum for C_2 species (10% CH_4, $T_s = 950$ °C, $P = 2.93$ kW) demonstrates good resolution of OES system. The (0-0) band head is marked on the right site. The numbers above each line denote the corresponding $J''(P_{22})$ numbers. $\Delta\lambda$ is the wavelength shift between (0-0) band edge and $P_{22}(J'' = 23)$ line. The horizontal dashed line shows the level of dark noise (830 counts) of the spectrometer.

region (horizontal cylinder with ≈10 mm diameter) of the plasma cloud using OES. Typical panoramic low-resolution OES spectra for CH_4 concentrations of 2% and 10% are shown in Fig. 11. The most prominent lines seen are the atomic hydrogen lines H_α (656.5 nm), H_β (486.1 nm), H_γ (434.1 nm) of Balmer series, four intensive dimer C_2 systems (471.5, 516.5, 563.2 and 619.1 nm) and the relatively weak CH band (431.4 nm and 432.4 nm) [46]. The atomic hydrogen lines strongly reduced with the adding of more methane in the plasma, while C_2 bands demonstrate the opposite tendency.

The gas temperature was evaluated from intensity of dimer C_2 Swan system ($d^3\Pi_g \rightarrow a^3\Pi_u$) in optical emission spectrum (band head at 516.5 nm) following the approach described by Gicquel et al. [30,31] and Hemawan et al. [46]. The $a^3\Pi_u$ state is metastable, while the $d^3\Pi_g$ level with energy 2.59 eV above the ground state, has a radiative lifetime of 120 ns [47,48]. Assuming a thermal equilibrium between rotational levels, the emission is linked to the rotational temperature T_{rot} through Boltzmann's relation. We used this method as it allows a rapid, direct and relatively accurate estimation of T_{rot}. An example of high resolution optical emission spectra is shown in Fig. 12.

The selected high resolution emission spectrum for C_2 species in Fig. 12 demonstrates quite good resolution in these measurements. To identify J number for each line in the spectrum we used the well known value $\Delta\lambda$ for the shift between (0-0) band head and selected line [49]. Assuming a thermal equilibrium between rotational levels, the emission intensities are linked to the rotational temperature through Boltzmann's relation:

$$I_{em} \sim S_{J'J''} \times \exp\left[\frac{-hcB'_vJ'(J'+1)}{k_BT_{rot}}\right] \quad (3)$$

where I_{em} is intensity of individual lines, J' is corresponding rotating values for upper states of this lines, $S_{J'J''}$ is the Hönl–London factor for this transition, $B_v^{'}$ is rotational momentum of C_2 molecule in upper state and k_B, c and h are Boltzmann's constant, the light speed and Plank's constant, respectively. The numerical values for $S_{J'J''}$ and $B_v^{'} = 1.755\ cm^{-1}$ were taken from [50,49], respectively. The plot $\ln(I_{em}/S_{J'J''})$ *vs* $J'(J'+1)$ gives the rotational temperature T_{rot} of the upper state of transition from the slope of linear fit [31]. We used a large number of the lines in the interval of J' from 24 to 47 to extend the energy range and, thus, to improve the accuracy in T_{rot}. For particular case of growth

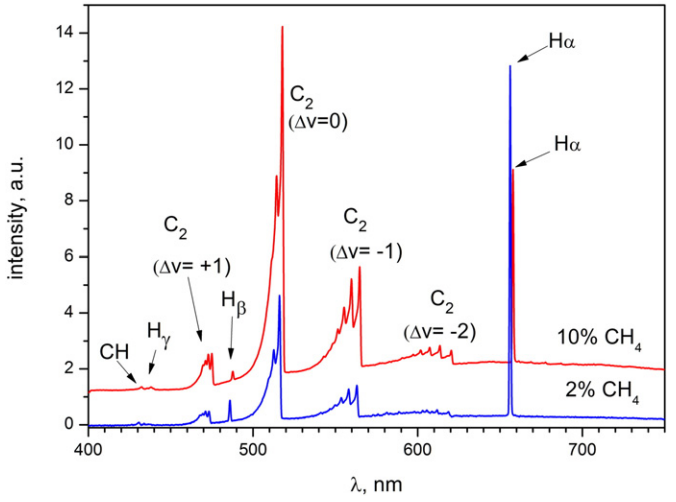

Fig. 11. Panoramic low resolution OES spectra of $H_2 + CH_4$ plasma for 2% and 10% CH_4 in the wavelength range of 400–700 nm. Growth conditions: $Q = 500$ sccm, $p = 130$ Torr, $P = 3.0$ kW. The spectra are shifted for clarity.

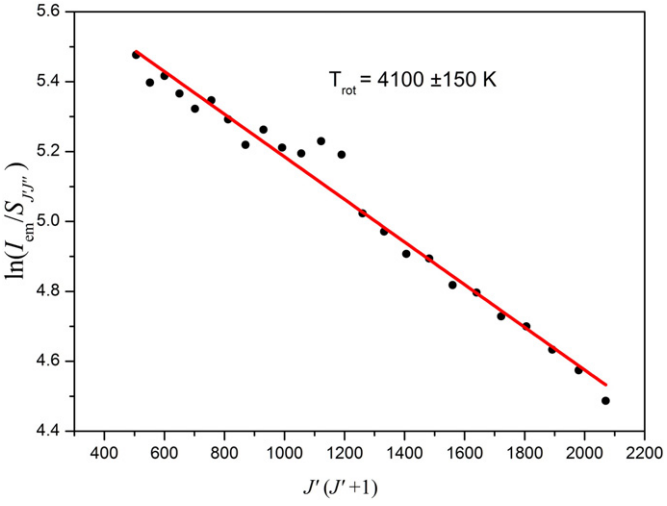

Fig. 13. Boltzmann's plot $\ln(I_{em}/S_{J'J''})$ *vs* $J'(J'+1)$ based on the data in Fig. 12 ($CH_4 = 10\%$, $P = 2.93$ kW). The circles are the experimental data, and the solid line is linear fit. The slop gives gas rotational temperature $T_{rot} = 4140 \pm 150$ K.

at $CH_4 = 10\%$, $P = 2.93$ kW (Fig. 13) the rotational temperature $T_{rot} = 4140 \pm 150$ K has been determined. The accuracy of 4% in T_{rot} was typical in such calculations.

We observed that the dependence of gas temperature in the core of plasma cloud on absorbed power for particular (fixed) CH_4 contents is weak over $P = 2.0$–3.3 kW, as seen in Fig. 10. The temperature T_{rot} is very stable (2900–3100 K) with absorbed MW power at 2% CH_4, and shows a slight increase from 3600 to 4200 K at higher (10%) CH_4 content in gas. This finding, coupled to similar conclusion on low sensitivity of MWPD to the absorbed power, indicates that the measured dependence of the diamond epitaxial growth rate is mainly due to substrate temperature effect on the surface chemistry, while the microwave power induced plasma chemistry plays a minor role in the growth kinetics. The measured significant increase in the gas temperature T_{rot} with methane concentration (compare 2% and 10% in Fig. 10) is in agreement with the trend obtained from the plasma simulation as reported by Hassouni et al. [51]. The extrapolated value for gas temperature difference between 1% and 10% CH_4 is $\Delta T \approx 120$ K in their simulation (see Fig. 14 in [51]), however, in our measurements the difference is much larger, up to 1000 K. One possible explanation of this discrepancy could be related to the fact, that the microwave power density was much lower in the simulation (about 10 W/cm^3) than in the present work (300–500 W/cm^3).

3.7. Sample characterization

A multistack (totally 61 layers) epitaxial diamond film, as shown schematically in Fig. 14, has been produced upon continuous growth with variable process parameters during approximately 7 h, with total CVD diamond thickness increment of 142 μm. The typical thickness of each layer varied from ≈100 nm for growth at low CH_4 content (1%) up to ≈10 μm at high (13%) CH_4 content in gas.

The surface relief of the terminate (top) layer, deposited at 13% CH_4, $T_s = 1117$ °C, was measured with AFM and is shown in Fig. 15. The relief is quite complex, displaying a number of features of different scales. Cylinder-like ridges of 20–30 μm in "diameter" with valleys of up to 0.5 μm

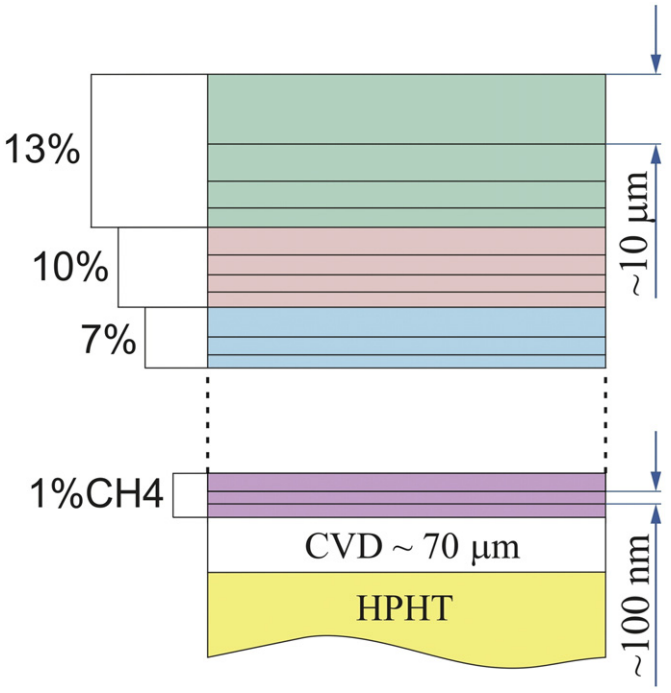

Fig. 14. Schematic view in cross section of a stack (totally 61 layers) epitaxial diamond film, sequentially grown on one substrate at different process parameters.

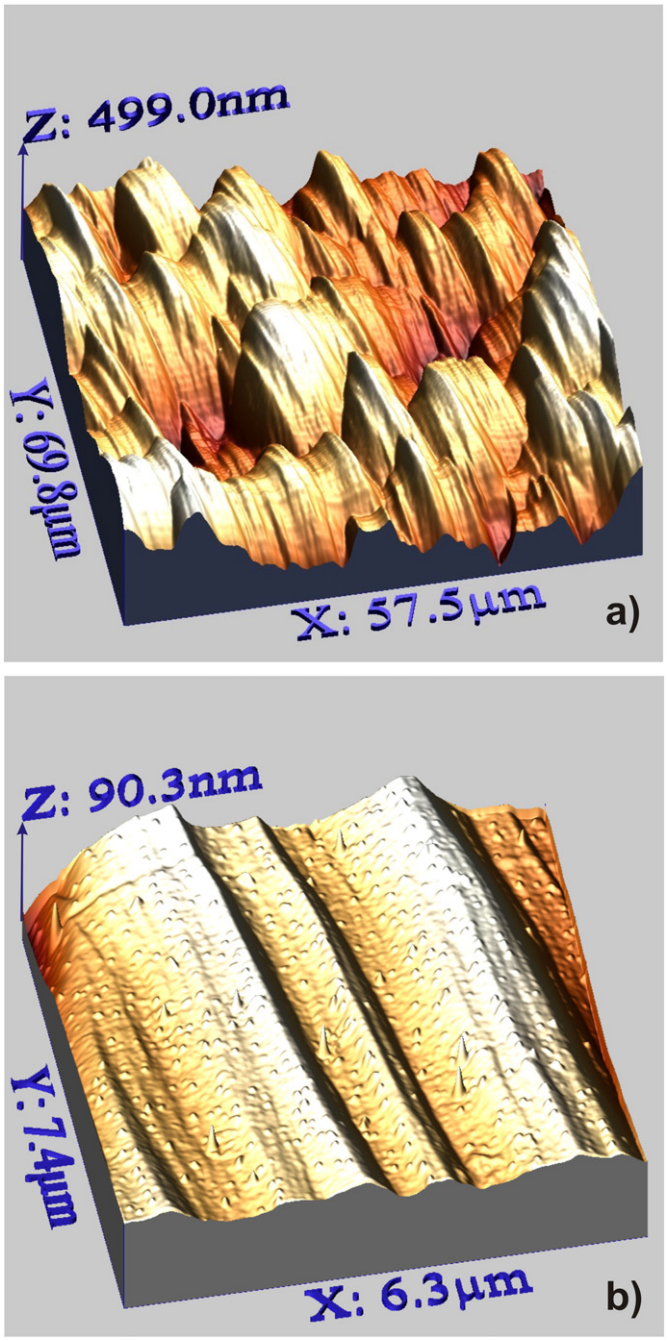

Fig. 15. AFM images of surface relief of the sample with a 9 μm thick terminate layer deposited at 13% CH_4 and $T_s = 1117$ °C (a); a detail of the same area (b).

deep in between, align along X-axis, each ridge being modulated with steps, oriented in Y-axis (Fig. 15a). The surface roughness is $R_a = 61$ nm on area of 70×57 μm^2. It was found with the optical profilometer that the long axis of the ridges is directed along [100] orientation. The terraces 1–2 μm wide and steps of up 70 nm in height are seen in more detail in Fig. 15b. The step growth is quite typical for diamond epitaxy, and the formation of the wide terraces suggests a large migration length of carbon species before being accommodated in diamond lattice [52]. The larger scale features ("bumps") presumably are result of superposition of different modes of growth for each layer beneath, that formed at the deposition conditions varied in a broad range. A similar surface relief was measured also with an optical profilometer on a larger area 177×133 μm^2, and the surface roughness $R_a \approx 86$ nm has been determined.

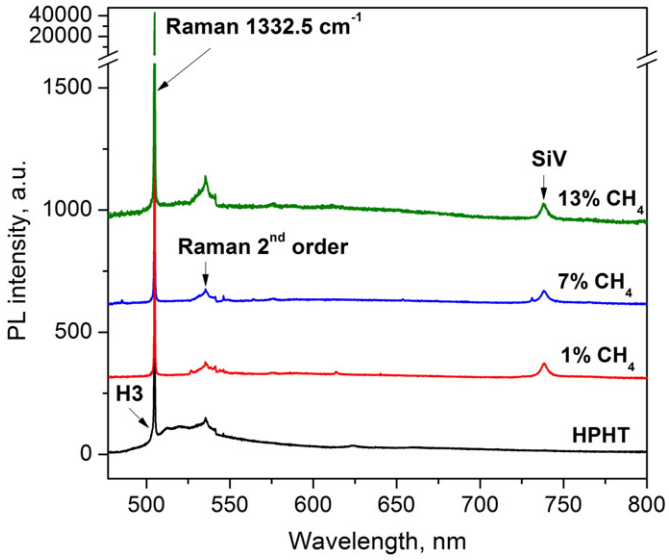

Fig. 16. PL spectra for diamond layers grown at 1%, 7% and 13% CH_4 in gas and for HPHT substrate. The spectra are taken in cross-section of the stack sample (see Fig. 14), and zoomed to enhance the PL features. The band between the 1st and 2nd order Raman peaks is phonon replicas of PL band of H_3 defect. The spectra are vertically shifted for clarity.

Raman and photoluminescence (PL) spectra were taken in polished cross-section on different layers to see how the material quality varies with methane concentration in process gas. Mapping of Raman spectrum across the depth of the grown stack was performed with a step of 1 μm. The diamond Raman peak width (full width at half magnitude) $\Delta\nu$ was found to be essentially constant, $\Delta\nu = 2.4 \pm 0.1$ cm^{-1} through all epilayers. For comparison, Raman peak width for a reference sample, natural IIa diamond, was 2.3 cm^{-1}, as measured in identical conditions.

Fig. 16 displays PL spectra for the diamond layers produced at different methane concentrations of 1%, 7% and 13% in gas. The PL features are very week relative to intensity of 1st order Raman peak for diamond at 1332.5 cm^{-1}, therefore the spectra have been zoomed to show the PL structure in more detail. Besides the strong 1st order Raman peak the 2nd order Raman peak at 535 nm and silicon-vacancy (SiV) PL band with zero-phonon line (ZPL) at 738 nm can be seen, the latter being formed due to contamination of the reactor chamber with Si in previous experiments. The intensity of SiV PL ZPL is ≈200 times less than that for Raman peak. For comparison, the PL spectrum for HPHT substrate is also shown (bottom spectrum in Fig. 16), that doesn't reveal SiV peak, but displays the H_3 line corresponding to nitrogen-vacancy complex defect N-V-N with ZPL at 503.4 nm, typical for HPHT diamonds. Very small neutral nitrogen-vacancy NV^0 peak could also be identified at 575 nm in the PL spectra for CVD diamond layers. Since the intensity of the NV^0 PL line is three orders of magnitude lower compared to that for 1st order Raman peak, the purity and crystallinity of the epilayers is rather high, in terms of Raman and PL spectroscopy evaluation, throughout the entire growth parameters explored.

4. Concluding remarks

We have demonstrated how effective the *in situ* monitoring of the growth rate of epitaxial single crystal diamond is in a microwave plasma CVD process when using low-coherence interferometry. The growth rate in H_2-CH_4 gas mixtures is measured in the wide temperature range of 750–1150 °C and in the wide methane content of 1–13% by preparing a stack with several tens layers on one (100) Ib type HPHT substrate without switching off the plasma. In some cases, the deposition of a layer as thin as 100 nm was enough to determine the growth rate. The accuracy of ≈0.4% in the reported growth rate is estimated, the substrate temperature fluctuations and drift being thought to ultimately limit the accuracy of the growth rate measurement by the present method. Potentially the accuracy can be further improved provided the substrate temperature is highly stabilized. The growth rate of as high as 82 μm/h is achieved by optimizing (increasing) the growth temperature. The *in situ* LCI technique dramatically reduces the time to collect kinetics data (typically 5–10 min for one growth regime), without spent of many substrates. All measurements described in the present paper were performed during one working day.

Activation energy $E_a = 11.1 \pm 1.0$ kcal/mol is determined for diamond growth at moderate and high CH_4 concentrations (7–13%), while activation energy $E_a = 9.8 \pm 0.8$ kcal/mol was found for etching in pure H_2. The etching has a strong effect on growth at low CH_4 contents, moreover, a transition from the growth to etching was observed at high enough substrate temperature (>1000 °C). The method allows a significant improvement in measurement accuracy of activation energy in comparison with the conventional approach (one regime – one sample) owing to collecting a vast array of growth rate data points. The accuracy of ≈10% in E_a obtained in the present work can be further improved using smaller temperature steps upon the growth rate measurement.

Rotation temperature T_{rot} for C_2 dimer was determined from analysis of Swan band $d^3\Pi_g \rightarrow a^3\Pi_u$ in optical emission spectra of the plasma, and it's found that the gas temperature remains relatively stable with variations of absorbed microwave power. Also, the absorbed power density demonstrates only a slight decrease with absorbed MW power, suggesting the plasma chemistry changes also small. Therefore, the substrate temperature control by MW power could be acceptable for study of temperature surface reactions kinetics.

Prime novelty

The growth rate of epitaxial single crystal diamond upon microwave plasma CVD in H_2-CH_4 gas mixtures is systematically measured *in situ* in a wide temperature (750–1150 °C) and methane content (1–15%) ranges with a low-coherence interferometry, using only a single HPHT substrate to form a multilayered film without switch-off the plasma. The method allows very quick and precise collection of kinetic data and optimizing the growth process.

Acknowledgments

The authors acknowledge S.G. Ryzhkov for the sample polishing, P.V. Volkov for expert assistance in LCI instrument performance, and E.V. Zavedeev for optical profilometry. This work was supported by Russian Science Foundation, grant no. 14-12-01403.

References

[1] M. Pomorski, C. Delfaure, N. Vaissiere, H. Bensalah, J. Barjon, M.A. Pinault-Thaury, D. Tromson, P. Bergonzo, Characterization of the charge-carrier transport properties of IIa-tech SC diamond for radiation detection applications, Phys. Status Solidi A 212 (2015) 2553–2558.
[2] T. Kononenko, A. Bolshakov, V. Ralchenko, V. Konov, P. Allegrini, M. Pacilli, G. Conte, E. Spiriti, An all-carbon detector with buried graphite pillars, Appl. Phys. A Mater. Sci. Process. 114 (2014) 297–300.
[3] R.P. Mildren, A. Sabella, O. Kitzler, D.J. Spence, A.M. McKay, Diamond Raman laser design and performance, in Optical Engineering of Diamond, in: R.P. Mildren, J.R. Rabeau (Eds.), Wiley-VCH Verlag 2013, pp. 239–276.
[4] R.S. Sussmann (Ed.), CVD Diamond for Electronic Devices and Sensors, John Wiley & Sons, Chichester, 2009.
[5] S. Shikata, Single crystal diamond wafers for high power electronics, Diam. Relat. Mater. 65 (2016) 168–175.
[6] I. Aharonovich, E. Neu, Diamond nanophotonics, Adv. Opt. Mater. 2 (2014) 911–928.
[7] J.E. Butler, Y.A. Mankelevich, A. Cheesman, J. Ma, M.N.R. Ashfold, Understanding the chemical vapor deposition of diamond: recent progress, J. Phys. Condens. Matter 21 (2009) 364201.
[8] Q. Liang, C.Y. Chin, J. Lai, C.S. Yan, Y. Meng, H.K. Mao, R.J. Hemley, Enhanced growth of high quality single crystal diamond by microwave plasma assisted chemical vapor deposition at high gas pressures, Appl. Phys. Lett. 94 (2009) 024103.

[9] J. Lu, Y. Gu, T.A. Grotjohn, T. Schuelke, J. Asmussen, Experimentally defining the safe and efficient, high pressure microwave plasma assisted CVD operating regime for single crystal diamond synthesis, Diam. Relat. Mater. 37 (2013) 17–28.
[10] A.B. Muchnikov, A.L. Vikharev, A.M. Gorbachev, D.B. Radishev, V.D. Blank, S.A. Terentiev, Homoepitaxial single crystal diamond growth at different gas pressures and MPACVD reactor configurations, Diam. Relat. Mater. 19 (2010) 432–436.
[11] F. Silva, K. Hassouni, X. Bonnin, A. Gicquel, Microwave engineering of plasma assisted CVD reactors for diamond deposition, J. Phys. Condens. Matter 21 (2009) 364202.
[12] N. Derkaoui, C. Rond, K. Hassouni, A. Gicquel, Spectroscopic analysis of H_2/CH_4 microwave plasma and fast growth rate of diamond single crystal, J. Appl. Phys. 115 (2014) 233301.
[13] J. Achard, A. Tallaire, R. Sussmann, F. Silva, A. Gicquel, The control of growth parameters in the synthesis of high-quality single crystalline diamond by CVD, J. Cryst. Growth 284 (2005) 396–405.
[14] A. Tallaire, C. Rond, F. Bénédic, O. Brinza, J. Achard, F. Silva, A. Gicquel, Effect of argon addition on the growth of thick single crystal diamond by high-power plasma CVD, Phys. Status Solidi A 208 (2011) 2028–2032.
[15] A.P. Bolshakov, V.G. Ralchenko, V.Y. Yurov, A.F. Popovich, I.A. Antonova, A.V. Khomich, I.I. Vlasov, E.E. Ashkinazi, S.G. Ryzhkov, A.V. Vlasov, A.A. Khomich, High rate growth of single crystal diamond in microwave plasma in H_2-CH_4 and H_2-CH_4-Ar mixtures in presence of intensive soot formation, Diam. Relat. Mater. 62 (2016) 49–57.
[16] C.S. Yan, Y.K. Vohra, H.K. Mao, R.J. Hemley, Very high growth rate chemical vapor deposition of single-crystal diamond, Proc. Natl. Acad. Sci. U. S. A. 99 (2002) 12523–12525.
[17] A. Tallaire, J. Achard, F. Silva, O. Brinza, A. Gicquel, Growth of large size diamond single crystals by plasma assisted chemical vapour deposition: recent achievements and remaining challenges, C. R. Phys. 14 (2013) 169–184.
[18] A. Chayahara, Y. Mokuno, Y. Horino, Y. Takasu, H. Kato, H. Yoshikawa, N. Fujimori, The effect of nitrogen addition during high-rate homoepitaxial growth of diamond by microwave plasma CVD, Diam. Relat. Mater. 13 (2004) 1954–1958.
[19] T. Teraji, Chemical vapor deposition of homoepitaxial diamond films, Phys. Status Solidi A 203 (2006) 3324–3357.
[20] J. Achard, F. Silva, O. Brinza, A. Tallaire, A. Gicquel, Coupled effect of nitrogen addition and surface temperature on the morphology and the kinetics of thick CVD diamond single crystals, Diam. Relat. Mater. 16 (2007) 685–689.
[21] H. Yamada, A. Chayahara, S. Ohmagari, Y. Mokuno, Factors to control uniformity of single crystal diamond growth by using microwave plasma CVD, Diam. Relat. Mater. 63 (2016) 17–20.
[22] E.V. Bushuev, V.Y. Yurov, A.P. Bolshakov, V.G. Ralchenko, E.E. Ashkinazi, A.V. Ryabova, I.A. Antonova, P.V. Volkov, A.V. Goryunov, A.Y. Luk'yanov, Synthesis of single crystal diamond by microwave plasma assisted chemical vapor deposition with in situ low-coherence interferometric control of growth rate, Diam. Relat. Mater. 66 (2016) 83–89.
[23] H. Watanabe, D. Takeuchi, S. Yamanaka, H. Okushi, K. Kajimura, T. Sekiguchi, Homoepitaxial diamond film with an atomically flat surface over a large area, Diam. Relat. Mater. 8 (1999) 1272–1276.
[24] S.G. Ri, H. Watanabe, M. Ogura, D. Takeuchi, S. Yamasaki, H. Okushi, Hydrogen plasma etching mechanism on (001) diamond, J. Cryst. Growth 293 (2006) 311–317.
[25] T. Shimaoka, J.H. Kaneko, M. Tsubota, H. Shimmyo, H. Watanabe, A. Chayahara, H. Umezawa, S.I. Shikata, High-performance diamond radiation detectors produced by lift-off method, Europhys. Lett. 113 (2016) 62001.
[26] Y. Gu, J. Lu, T. Grotjohn, T. Schuelke, J. Asmussen, Microwave plasma reactor design for high pressure and high power density diamond synthesis, Diam. Relat. Mater. 24 (2012) 210–214.
[27] A. Tallaire, J. Achard, F. Silva, R.S. Sussmann, F. Gicquel, E. Rzepka, Oxygen plasma pre-treatments for high quality homoepitaxial CVD diamond deposition, Phys. Status Solidi A 201 (2004) 2419–2424.
[28] M. Naamoun, A. Tallaire, F. Silva, J. Achard, P. Doppelt, A. Gicquel, Etch-pit formation mechanism induced on HPHT and CVD diamond single crystals by H_2/O_2 plasma etching treatment, Phys. Status Solidi A 209 (2012) 1715–1720.
[29] J. Ma, M.N.R. Ashfold, Y.A. Mankelevich, Validating optical emission spectroscopy as a diagnostic of microwave activated $CH_4/Ar/H_2$ plasmas used for diamond chemical vapor deposition, J. Appl. Phys. 105 (2009) 043302.
[30] X. Duten, A. Rousseau, A. Gicquel, P. Leprince, Rotational temperature measurements of excited and ground states of C_2 ($d^3\Pi_g$ - $a^3\Pi_u$) transition in a H_2/CH_4 915 MHz microwave pulsed plasma, J. Appl. Phys. 86 (1999) 5299–5301.
[31] G. Lombardi, F. Bénédic, F. Mohasseb, K. Hassouni, A. Gicquel, Determination of gas temperature and C_2 absolute density in $Ar/H_2/CH_4$ microwave discharges used for nanocrystalline diamond deposition from the C_2 Mulliken system, Plasma Sources Sci. Technol. 13 (2004) 375–386.
[32] W.J. Tropf, M.E. Thomas, M.J. Linevsky, Infrared refractive indices and thermooptic coefficients for several materials, Proc. SPIE 3425 (1998) 160–171.
[33] T. Ruf, M. Cardona, C.S.J. Pickles, R. Sussmann, Temperature dependence of the refractive index of diamond up to 925 K, Phys. Rev. B 62 (2000) 16578–16581.
[34] G.A. Slack, J. Bartram, Thermal expansion of some diamondlike crystals, J. Appl. Phys. 46 (1975) 89–98.
[35] C.C. Battaile, D.J. Srolovitz, I.I. Oleinik, D.G. Pettifor, A.P. Sutton, S.J. Harris, J.E. Butler, Etching effects during the chemical vapor deposition of (100) diamond, J. Chem. Phys. 111 (1999) 4291–4299.
[36] H. Maeda, K. Ohtsubo, M. Irie, N. Ohya, K. Kusakabe, S. Morooka, Determination of diamond [100] and [111] growth rate and formation of highly oriented diamond film by microwave plasma-assisted chemical vapor deposition, J. Mater. Res. 10 (1995) 3115–3123.
[37] C.J. Chu, R.H. Hauge, J.L. Margrave, M.P. D'evelyn, Growth kinetics of (100), (110), and (111) homoepitaxial diamond films, Appl. Phys. Lett. 61 (1992) 1393–1395.
[38] R.A. Weimer, T.P. Thorpe, K.A. Snail, Growth rate and quality variation of homoepitaxial diamond grown at elevated temperatures, J. Appl. Phys. 77 (1995) 641–645.
[39] A. Cheesman, J.N. Harvey, M.N.R. Ashfold, Studies of carbon incorporation on the diamond {100} surface during chemical vapor deposition using density functional theory, J. Phys. Chem. A 112 (2008) 11436–11448.
[40] J.E. Butler, A. Cheesman, M.N.R. Ashfold, Recent progress in the understanding of CVD growth of diamond, in: R.S. Sussmann (Ed.), CVD Diamond for Electronic Devices and Sensors, John Wiley & Sons, Chichester 2009, pp. 103–124.
[41] O.A. Ivanov, A.B. Muchnikov, V.V. Chernov, S.A. Bogdanov, A.L. Vikharev, J.E. Butler, Experimental study of hydrogen plasma etching of (100) single crystal diamond in a MPACVD reactor, Mater. Lett. 151 (2015) 115–118.
[42] K. Hassouni, G. Lombardi, X. Duten, G. Haagelar, F. Silva, A. Gicquel, T.A. Grotjohn, M. Capitelli, J. Ropcke, Overview of the different aspects in modelling moderate pressure H_2 and H_2/CH_4 microwave discharges, Plasma Sources Sci. Technol. 15 (2006) 117–125.
[43] A. Gicquel, K. Hassouni, Y. Breton, M. Chenevier, J.C. Cubertafon, Gas temperature measurements by laser spectroscopic techniques and by optical emission spectroscopy, Diam. Relat. Mater. 5 (1996) 366–372.
[44] K. Hameurlaine, Contribution to the Study of a Lower Power Electric Arc(Thesis) Université D'Orléans, Orleans, 2012 116.
[45] M.A. Lobaev, S.A. Bogdanov, D.B. Radishev, A.L. Vikharev, A.M. Gorbachev, Method of power density determination in microwave discharge, sustained in hydrogen–methane gas mixture, Diam. Relat. Mater. 66 (2016) 177–182.
[46] K.W. Hemawan, R.J. Hemley, Optical emission diagnostics of plasmas in chemical vapor deposition of single-crystal diamond, J. Vac. Sci. Technol. A 33 (2015) 061302.
[47] T. Tatarczyk, E.H. Fink, K.H. Becker, Lifetime measurements on single vibrational levels of C_2 ($d^3\Pi_g$) by laser fluorescence excitation, Chem. Phys. Lett. 40 (1976) 126–130.
[48] T. Wakasaki, K. Sasaki, K. Kadota, Collisional quenching of $C_2(d^3\Pi_g)$ and $C_3(\tilde{A}^1\Pi_u)$ and its application to the estimation of absolute particle density in laser-ablation carbon plumes, Jpn. J. Appl. Phys. 41 (2002) 5792–5796.
[49] C.V.V. Prasad, P.F. Bernath, Fourier transform spectroscopy of the Swan ($d^3\Pi_g$-$a^3\Pi_u$) system of the jet-cooled C_2 molecule, Astrophys. J. 426 (1994) 812–821.
[50] L.L. Danylewych, R.W. Nicholls, Intensity measurements on the C_2 ($d^3\Pi g$-$a^3\Pi_u$) Swan band system. I. Intercept and partial band methods, Proc. R. Soc. Lond. A 339 (1974) 197–212.
[51] K. Hassouni, O. Leroy, S. Farhat, A. Gicquel, Modeling of H_2 and H_2/CH_4 moderate-pressure microwave plasma used for diamond deposition, Plasma Chem. Plasma Process. 18 (1998) 325–362.
[52] T. Teraji, S. Mitani, T. Ito, High rate growth and luminescence properties of high-quality homoepitaxial diamond (100) films, Phys. Status Solidi A 198 (2003) 395–406.